Article

Energy Flux Method for Wave Energy Converters

Gabriel Thomas Scarlett [1], James Cameron McNatt [1], Alan Henry [2] and Abel Arredondo-Galeana [3,*]

1   Mocean Energy Ltd., Murchison House, King's Buildings, Edinburgh EH9 3BF, UK;
    gabriel.scarlett@mocean.energy (G.T.S.); cameron.mcnatt@mocean.energy (J.C.M.)
2   Rockall Research Ltd., Sutton, D13 Dublin, Ireland; alan.henry@rockallsolutions.com
3   Department of Naval Architecture, Ocean & Marine Engineering, University of Strathclyde,
    Glasgow G4 0LZ, UK
*   Correspondence: abel.arredondo-galeana@strath.ac.uk

Abstract: Hydrodynamic tools reveal information as to the behaviour of a device in the presence of waves but provide little information on how to improve or optimise the device. With no recent work on the transfer of power (energy flux) from a wave field through the body surface of a wave energy converter (WEC), we introduce the energy flux method to map the flow of power. The method is used to develop an open-source tool to visualise the energy flux density on a WEC body surface. This energy flux surface can also be used to compute the total power capture by integrating over the surface. We apply the tool to three WEC classes: a heaving cylinder, a twin-hulled hinged barge, and pitching surge devices. Using the flux surfaces, we investigate power efficiency in terms of power absorbed to power radiated. We visualise the hydrodynamic consequence of sub-optimal damping. Then, for two pitching surge devices with similar resonant peaks, we reveal why one device has a reduced power performance in a wave spectrum compared to the other. The results show the effectiveness of the energy flux method to predict power capture compared to motion-based methods and highlight the importance of assessing the flux of energy in WECs subjected to different damping strategies. Importantly, the tool can be adopted for a wide range of applications, from geometry optimisation and hydrodynamic efficiency assessment to structural design.

Keywords: wave energy flux; wave energy converter; wave power

1. Introduction

A resurgence in wave energy development is underway in the UK, partly due to the Wave Energy Scotland (WES) stage program, which supports new developers in delivering cost-effective and reliable technologies [1]. To further improve early-stage development processes, the WEC.0 project was conceived, which is a consortium of technology developers who aim to develop tools for early-stage performance and cost design [2]. The work herein, which is part of the WEC.0 project, presents a new method for early-stage performance design.

State-of-the-art hydrodynamic tools reveal information as to the behaviour of a device in the presence of waves but provide little information on how to improve or optimise the device. We ask whether existing tools can be used to develop a new method to both map and visualise the flow of power, or energy flux, through the hull surface of a WEC. This would reveal the portions of the hull that absorb power and to what degree, as well as portions of the hull that experience force but do not absorb power. It is hoped that this will offer a new fast method to aid iterative design and optimisation.

1.1. Wave Energy Absorption

The choice of the surface over which to understand the flow of wave energy in the context of wave energy converters (WECs) divides the theoretical understanding of wave energy absorption into two groups, which Falnes and Kurniwan [3] describe as a Local

Point of View (LPV), known as the near field, and a Global Point of View (GPV), referred to as the far field. The LPV considers power absorption through the body surface of WECs. Fluid pressure integrated over the body surface results in forces on the WEC, which are formed as part of an equation of motion and an equation for power absorption. Therefore, the equations in the LPV relate to the forces on and motions of a WEC. In contrast, the GPV considers a control surface in the fluid domain, typically encompassing a WEC or an array of WECs. The GPV describes the flow of energy through the wave field, frequently expressing the flow of energy in terms of an incident (or incoming) wave, and waves that propagate away from the WEC or WEC array, which either transport energy or act to cancel out portions of the incoming wave, representing energy absorption. The equations in the GPV relate to the waves incoming to the WEC and those radiated or scattered by the WEC.

The following literature review is carried out in the context of LPV and GPV perspectives on wave energy absorption and the relationship between the two.

1.2. Wave Relationships

Early theoretical wave energy research [4–7] focuses on the relationship between the LPV and GPV. In fact, many early papers use forces evaluated from wave radiation patterns (GPV). Because the connections between the LPV force and GPV wave patterns were important to these early works, they are discussed here first.

Green's Theorem is a relationship that when applied to the velocity potentials $\phi^{(1)}$ and $\phi^{(2)}$ results in the following relationship (c.f. [8] Section 3.5):

$$\iint_S \left(\phi^{(1)} \frac{\partial \phi^{(2)}}{\partial n} - \phi^{(2)} \frac{\partial \phi^{(1)}}{\partial n} \right) dS = 0, \tag{1}$$

where $\phi^{(1)}$ and $\phi^{(2)}$ are potential functions that are solutions to the Laplace equation in a volume of fluid V, which is bounded by a surface S; dS is an infinitesimal element of surface S; and n denotes the normal direction to S and points into the fluid [9].

It is from Green's theorem that, by selecting the appropriate pairs of velocity potentials, the so-called Haskind relation (see [4]) and others are derived. In the Haskind relation, the wave excitation force in degrees of freedom (DOF) i on a body is found via a formula that considers only the far-field radiation pattern of motion in DOF j. The relationship is derived by noting that, for the velocity potentials under consideration, the term in parenthesis in Equation (1) is zero everywhere except on the body surface and on the control surface surrounding the body. This means that the integrals of the velocity potential over a control surface within the wave field can be used to evaluate integrals over the body surface. That is, the LPV forces are connected to the GPV wave field patterns.

Newman [4] applies this relationship to compute the wave excitation forces on ellipsoids, for which the wave radiation patterns can be described analytically. He then goes on to demonstrate a relationship between the damping coefficients of a floating body and the integral of the wave excitation force over all incident angles. Later, Newman [5] systematically works through relationships that arise out of Green's Theorem. This work reveals well-known and useful relations based on the far-field (i.e., GPV) wave pattern and shows several new ones related to wave energy.

1.3. Early Wave Energy Literature

In a seminal paper on wave energy, Salter [10] derives the equation for wave energy flux per unit crest width for regular and irregular waves in deep water. He then uses this as a basis to describe the efficiency of WECs he tested physically, where efficiency is measured as the percentage of energy absorbed by the WEC from a wave frontage of width equal to that of the WEC. For tests undertaken on a pitching flap, Salter noted "an efficiency of about 40% ... Roughly 25% of the energy is transmitted onwards, and about 20% is transmitted back to the source". Realising that radiating a wave in the lee of the WEC results in uncaptured wave energy, Salter designed the Duck so that it did not displace

water astern, and measured efficiencies of over 80%. His approach is a GPV on WEC efficiency measured experimentally.

While Salter considers efficiency from a 2D perspective, Budal and Falnes [6] discuss a point-absorber-type WEC; that is, a small body in a much larger 3D domain. Taking an LPV, they note "… at resonance, the movement of the oscillator is in phase with the dynamic pressure of the incoming wave, resulting in a substantial transfer of energy from the wave to oscillator", and provide a formula for optimal power absorption in terms of the WEC's wave radiation damping value. However, they extend their analysis to a GPV, defining a so-called "absorption length", which is the width of wave frontage that is absorbed by a WEC, which is independent of the width of the WEC; note that absorption lengths wider than the WEC's diameter are possible. Furthermore, in experiments, they note observing an interesting GPV phenomenon of destructive wave interference, implying power absorption.

Providing more mathematics than previous work, Mei [11] begins with a theoretical basis for wave energy extraction from an LPV. His work starts with a formulation for power absorption based on an equation of motion that includes hydrodynamic forces. He shows that for optimal energy extraction, the WEC's power take-off (PTO) damping must be equal to the wave radiation damping and that the WEC should be kept in resonance. He then connects the formulation to the GPV by relating the hydrodynamic forces to the waves radiated by the WEC using the Haskind relation. The equations are developed for a 2D domain and for WECs with 1 and 2 DOF.

Evans [7] provides a more extensive theory for the analysis of WECs based on the linear WAVE–BODY BOUNDARY VALUE PROBLEM and covers many of the same aspects as Mei [11]. Like Mei, the hydrodynamic forces in his equation of motion are based on the radiated waves using the Haskind relation (providing a connection between the LPV and the GPV). He develops an equation for efficiency in 2D based on two key parameters, one of which depends on body motions, while the other is independent of body motions but dependent on geometry. By considering the geometry parameter, he notes a condition consistent with Salter's design for the Duck: "a highly efficient cylinder" only radiates waves in the opposite direction of the incoming waves. He considers the problem in 3D and derives fundamental relationships for the absorption length (a term coined by Budal and Falnes [6]) for a small body moving in heave. Notably, Evan's pioneering work on submerged cylinders form the basis of a device later referred to as the Bristol Cylinder [12–14].

In the first work to consider WEC arrays, in a theoretical context, Budal [15] provides an equation for the power absorbed by a WEC array as the time average product of the fluid pressure and fluid velocity on the total wetted surface of all bodies in the array (a LPV). To further his analysis, using Green's Theorem, he transforms the equation for power into one based on the far-field fluid motions (a GPV). He defines power absorption in terms of the absorption length of the array and also defines a widely used measure for array performance, known as the q-factor, which is the ratio of power absorption by the array to the power absorption by an equivalent number of isolated single WECs.

1.4. Recent Wave Energy Literature

Folley [16] is the editor of a recently published textbook called *Numerical Modelling of Wave Energy Converters*, sections of which are written by prevailing experts in wave energy. It contains a comprehensive overview of state-of-the-art practical numerical WEC modelling techniques including frequency-domain potential flow, linear time-domain potential flow, quasi-nonlinear time-domain methods, so-called spectral-domain techniques, nonlinear potential flow, and computational fluid dynamics models. Equations for optimal power are covered, which include hydrodynamic parameters. However, power absorption by WECs is generally considered through the product of force and velocity in the mechanical PTO system. That is, even when considering the equations for optimal power absorption, modern practical methods of evaluating WEC power rely on an LPV approach. Wave forces

are computed using fluid models; these are applied within an equation of motion that includes mechanical forces to derived body motions and PTO power generation, which are then used to compute power. There is no consideration of the power flow through the wave field either near the WEC or in the far field. Nevertheless, other authors have considered power absorption in terms of a GPV from a theoretical perspective.

Wypych et al. [17] use the solutions to the linear wave boundary value problem in cylindrical coordinates to represent the waves radiated by heaving and surging point absorbers. Their solution is exact throughout the wave field (rather than only being applicable in the far field, as was the case with previous authors); power is computed as flux through a cylindrical control surface in the wave field at an arbitrary radius (a GPV), and the results agree with previously derived theoretical results for point absorbers. In addition, they present results from experiments that show that the radiated waves of a heaving or surging sphere agree with linear theory, except for high-order harmonics, which would represent a loss in a WEC system.

Stansell and Pizer [18] consider the theory of energy absorption by a line absorber (also frequently called an attenuator) as a line of point absorbers. They formulate an equation for power absorption as a surface integral over the body expressed as the product of pressure and velocity, and then use Green's Theorem to convert the power integral over the body to an integral over a far-field cylindrical control surface (i.e., a conversion from a LPV to a GPV), which results in a compact expression for average absorbed power. They note that line absorbers incorporate extra degrees of freedom beyond point absorbers, which enable them to focus their radiated wave and absorb more energy.

The final paper discussed here is that of Falnes and Kurniawan [3], already touched upon at the beginning of the literature review to introduce the terminology of the local point of view (LPV) and global point of view (GPV), a set of perspectives that guides the work. They systematically work through equations for power absorption for each point of view, generalising the theory to include arrays and oscillating water columns. Their GPV work includes formulae using both radiated and scattered waves and radiated waves alone, addressing discussions as to whether it is the forward or the aft travelling generated wave that is fundamental to absorbing power. They point out that while both the LPV and GPV are capable of describing the average power absorption, only the LPV can be used to compute instantaneous power absorption, which is relevant when considering reactive power. Falnes and Kurniawan nicely tie together LVP and GVP in a comprehensive set of formulae.

1.5. Synthesis of Literature Review

It is clear from early theoretical [4,5,7,11] and practical work [6,10] on wave energy absorption that there is a direct connection between wave forces on and the power absorption of a WEC and the waves generated by that body (an LPV to GPV relationship). In fact, theoretical works rely on far-field wave patterns to compute wave forces and power absorption [4,5,7,11,13,15,19]. These early works consider idealised cases where WECs generate waves of any amplitude, which results in the 3D energy absorption of wave frontages wider than the WEC's width [7,13,15]. Later works observe that the amplitude of body motions required to achieve these waves is, in some cases, unphysical, and so their work addresses practical constraints, which results in smaller levels of power absorption [14,19–21]. Although some recent work considers wave energy absorption through the wave field in a GPV, it is theoretical [17,18], and state-of-the-art practical methods for computing wave energy absorption by WECs use numerically computed wave forces within an equation of motion to compute mechanical power [16,22–24].

We, therefore, ask the following question: is there a practical way to assess, understand, and/or visualise the flow of power through the wave field to the moving body that could improve the understanding, design, and performance of WECs?

1.6. Overview and Layout of Paper

In the remainder of this paper, we develop a method to visualise the flow of energy through the wave field to the moving body. This "energy flux" method aims to map the flow of power from the wave field to a WEC in order to aid in the understanding of the WEC's performance and behaviour. The terminology 'flow of energy' used here is synonymous with power.

The remaining structure of this manuscript is laid out as follows. In Section 2 (Materials and Methods), we present the theory relating the mechanical power in a moving body to the power passing through the body from the wave field, i.e., energy flux theory. Subsequently, we introduce the linear wave considerations used in this work. In Section 3 (Results), we use the open-source energy flux tool to illustrate and compare energy flux surface on a heaving cylinder, a hinged barge geometry with varying damping coefficients, and to compare two different pitching flap geometries. Then, in Section 4 (Discussion), the results and novelty of the method are discussed. Finally, in Section 5 (Conclusions), the main outcomes from this work are summarised, and suggestions for future work are given.

2. Materials and Methods

The following presents the materials and methods used in this manuscript. First, we introduce the theory relating the mechanical power in a WEC system to the power passing through the WEC's wetted surfaces in the wave field. It begins with the general relationship between mechanical power in a system and the power imparted by the fluid acting over the system's surfaces. The assumptions of linear wave theory are subsequently applied, and equations are decided on for the surface power (energy flux) in terms of the pressure force and velocity.

2.1. Energy Flux Theory

Power (P) in a mechanical system is the sum, in each DOF, j, of the product of force (F_j) and velocity (V_j), given as

$$P = \sum_j F_j V_j. \tag{2}$$

The force imparted by a fluid to that mechanical system is due to the pressure and shear stress acting over the surfaces of the system, defined as

$$F_j = \iint_S (p\mathbf{n} + \boldsymbol{\tau}) \cdot \mathbf{n_j} \, dA, \tag{3}$$

where S is the surface over which the forces act, p is the pressure, $\mathbf{n}$ is the surface normal, $\boldsymbol{\tau}$ is the shear stress on the surface, $\mathbf{n_j}$ is the unit normal vector that defines the direction of the motion of the DOF j, and A is the surface area.

Substituting Equation (3) into Equation (2) and rearranging the terms gives

$$P = \iint_S \sum_j (p\mathbf{n} + \boldsymbol{\tau}) \cdot V_j \mathbf{n_j} \, dA, \tag{4}$$

which can be written as

$$P = \iint_S dP, \tag{5}$$

where

$$dP = \sum_j (p\mathbf{n} + \boldsymbol{\tau}) \cdot V_j \mathbf{n_j} \, dA, \tag{6}$$

is an infinitesimal power or "surface power", composed of the product of an infinitesimal force and the velocity of the surface at that point.

Equations (5) and (6) are the essence of the energy flux theory. They state simply that the power imparted by a fluid to a system is the integral of surface power over the system's

surface, where the surface power is the product of infinitesimal force and velocity at each point. Equations (5) and (6) give the power and surface power as a function of time (*t*). The average surface power, which is often of most interest, is in DOF *j* for a time period *T*:

$$d\bar{P}_j = \frac{1}{T} \int_0^T dP_j(t)\, dt, \tag{7}$$

where

$$dP_j = (p\mathbf{n} + \boldsymbol{\tau}) \cdot V_j\mathbf{n_j}\, dA. \tag{8}$$

If the values in Equation (8) can be found explicitly for all points in time and space using numerical or experimental methods, then the surface power and average surface power can be found directly.

2.2. Linear Wave Theory

We adopt the assumptions of linear wave theory [4]. The assumption of an inviscid fluid means that the shear stress is zero. The assumptions of a linearised free surface and small body motions result in a wetted surface that is constant with time. This means that the body coordinates are equivalent to global coordinates (*n* and n_j are time-independent). Equation (8) becomes

$$dP_j = p(t)\mathbf{n} \cdot V_j(t)\mathbf{n_j}\, dA, \tag{9}$$

where only dP_j, *p*, and V_j are functions of time. In linear wave theory, the total pressure is the sum of the hydrostatic pressure over the mean body surface, p^{HS}, pressure, the diffracted wave, p^D, pressure, and radiated waves coming as a result of motions in each DOF, p_j^R, and the change in hydrostatic pressure due to motions, p_j^{dHS}.

$$p = p^{HS} + p^D + \sum_j (p_j^R + p_j^{dHS}). \tag{10}$$

The diffracted wave is the sum of the incident, p^I and the scattered, p^S pressures:

$$p^D = p^I + p^S. \tag{11}$$

The hydrostatic pressure on the mean surface is independent of time and is defined as

$$p^{HS} = -\rho g z. \tag{12}$$

The pressure as a function of time can be written as the inverse Fourier transform of frequency-domain representations as

$$p^{(D,R,dHS)}(t) = \Re \int_0^\infty \tilde{p}^{(D,R,dHS)}(\omega)e^{i\omega t} d\omega, \tag{13}$$

where ω is the angular wave frequency. Furthermore, the diffracted pressure can be written as the product of an incident wave amplitude and a unit pressure as follows:

$$p^D(t) = \Re \int_0^\infty \int_{-\pi}^\pi [a(\omega,\beta)\tilde{p}^D d\beta]e^{i\omega t} d\omega, \tag{14}$$

where β is the wave direction. Furthermore, the sum of the radiated pressure and delta hydrostatic pressure can be written as the product of the body motion amplitude and the pressure response to a unit amplitude motion as follows:

$$p_j^{\mathrm{R}}(t) = \Re \int_0^\infty \tilde{x}_j(\omega)(\hat{p}_j^{\mathrm{R}} + \hat{p}_j^{\mathrm{dHS}})(\omega)e^{i\omega t}\mathrm{d}\omega, \tag{15}$$

where the body motion amplitude ($\tilde{x}_j$) is found as the Fourier transform of the body motion time-domain signal:

$$\tilde{x}_j(\omega) = \Re \int_0^\infty X_j(t)e^{i\omega t}\mathrm{d}t. \tag{16}$$

Finally, the total pressure in the frequency domain is

$$\tilde{p}(\omega) = \int_{-\pi}^{\pi} a(\omega, \beta)\tilde{p}^{\mathrm{D}}(\omega, \beta)\mathrm{d}\beta + \sum_j \tilde{x}_j(\omega)(\hat{p}^{\mathrm{R}}(\omega) + \hat{p}^{\mathrm{dHS}}), \tag{17}$$

and Equation (9) becomes

$$\mathrm{d}P_j(t) = \left(\Re \int_0^\infty \tilde{p}(\omega)e^{i\omega t}\mathrm{d}\omega\right) V_j(t)\mathbf{n} \cdot \mathbf{n_j}\mathrm{d}A. \tag{18}$$

The average power can then be found from Equations (7) and (18) if one knows the incident wave amplitudes, $a(\omega, \beta)$, frequency-domain radiated, $\hat{p}_j^{\mathrm{R}}(\omega)$, diffracted pressures, $\hat{p}^{\mathrm{D}}(\omega, \beta)$, time-domain motions, $X_j(t)$, and velocities, $V_j(t)$.

However, instead of the time-domain motions and velocities, one may have the frequency-domain motions, $\tilde{x}_j(\omega)$, and velocities. Like the pressure, the time-domain velocity signal can be represented as the inverse Fourier transform of a frequency-domain signal as follows:

$$V_j(t) = \Re \int_0^\infty \tilde{v}_j(\omega)e^{i\omega t}\mathrm{d}\omega. \tag{19}$$

and Equation (18) becomes

$$\mathrm{d}P_j(t) = \left(\Re \int_0^\infty \tilde{p}(\omega)e^{i\omega t}\mathrm{d}\omega\right) \left(\Re \int_0^\infty \tilde{v}_j(\omega)e^{i\omega t}\mathrm{d}\omega\right)\mathbf{n} \cdot \mathbf{n_j}\mathrm{d}A. \tag{20}$$

If the solutions arise from the frequency domain, it means that the time over which the average is computed, T, goes to infinity. Thus, the cross terms in the product of pressure and velocity at different ω become zero, and the average power integral becomes

$$\mathrm{d}\bar{P}_j = \frac{1}{2}\Re \int_0^\infty \tilde{p}(\omega)\tilde{v}_j^*(\omega)\mathrm{d}\omega\,\mathbf{n} \cdot \mathbf{n_j}\,\mathrm{d}A, \tag{21}$$

where * denotes the complex conjugate.

3. Results

In this Section, the energy flux model is applied to three cases: heaving cylinder, hinged barge, and pitching flaps. Note that the energy flux model can be used to visualise the flow of power through the wave field to the moving body and also to compute power capture of the device. The tool is open-source and can be downloaded from our MWave GitHub repository [25] along with example files. MWave, originally developed as an interface for WAMIT, can compute WEC motions, power, wave fields, and more.

The model computes the power and surface power of the WEC with Equations (5) and (6), respectively, and the energy flux in the frequency domain given by Equation (21). The frequency domain solution is determined using the boundary element method (BEM) solver, WAMIT [26–29]. In WAMIT velocity potentials on the body and in the wave field are solved numerically using linear potential flow theory, where the fluid is assumed to be inviscid, the flow is assumed to be irrotational, and the amplitudes and body motions are assumed to be small, relative to wave length and body dimensions, respectively.

3.1. Heaving Cylinder

The first type of WEC analysed in this work was a heaving cylinder. The energy flux implementation was evaluated by comparing power capture prediction against a body motion power prediction. A simple heaving cylinder with measurements of 10 m in diameter, 12 m in height, and 10 m in draft was used. The full cylinder is shown in Figure 1a, and the wetted surface on which the energy flux was computed is shown in (b) along with the normal vectors. The orientation of the normals was important since we assumed that the absorbed power was positive in the direction of the normal (out of the body).
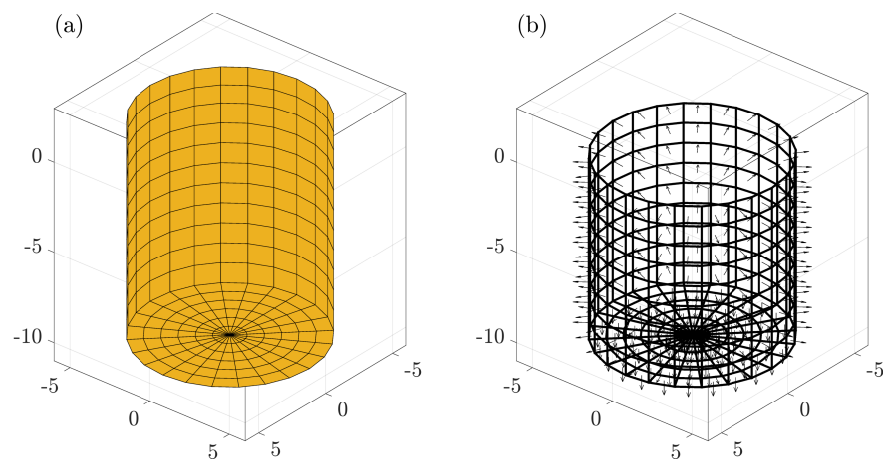
Figure 1. Cylindrical geometry showing (**a**) complete body mesh and (**b**) wetted flux surface mesh with normal vectors pointing outwards.

For a single PTO DOF, the average power absorbed by a WEC in the frequency domain is

$$\bar{P} = \frac{1}{2}\omega^2 d_{\mathrm{PTO}}|\zeta_{\mathrm{PTO}}|^2,　\tag{22}$$

where d_{PTO} and ζ_{PTO} are the PTO damping coefficient and complex-valued damped motion, respectively. The power RAO for the cylinder shown in Figure 2 for regular wave periods was $T \in [4, 12]$ s with $d_{\mathrm{PTO}} = 7$ MN/m applied to the heave motion, which was determined by maximising the peak power. A maximum of 220 kW/m^2 occured at $T = 7.4$ s.

Energy flux surfaces during a monochromatic wave with $T = 7.4$ s are shown in Figure 3 for (a) diffracted wave field (where the body is held still), (b) total (diffracted and radiated) wave field without PTO damping, and (c) PTO damping. Figure 3d shows the average energy flux surface with PTO damping, during an irregular wave of significant wave height, $H_s = 3.5$ m, and during a peak period, $T_p = 7.5$ s, which was modelled using a Bretschnider spectrum. The diffracted flux surface (a) is zero everywhere since the cylinder is held still so that there is no fluid–structure interaction. For case (b), we observe energy absorption on the near-side of the surface (denoted by a negative flux); however, since there is no PTO damping, the absorbed energy is fully radiated (see positive flux) on the far side and hence there should be zero net power. For cases (c) and (d), it is clear that there is a greater region of energy absorption than radiation, so there is net power in the system.
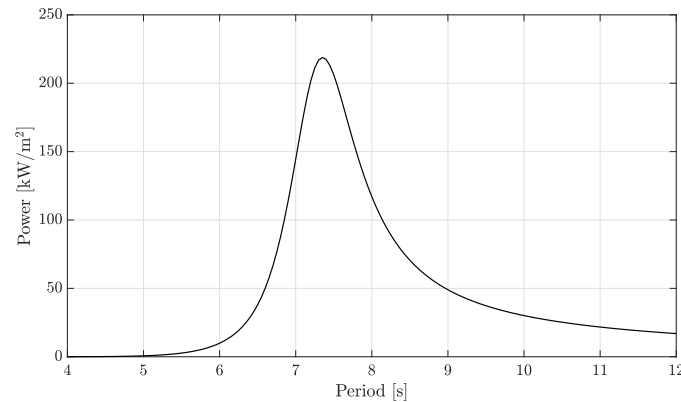
Figure 2. Power RAO for an optimum damping coefficient of 7 MN/m applied in heave.
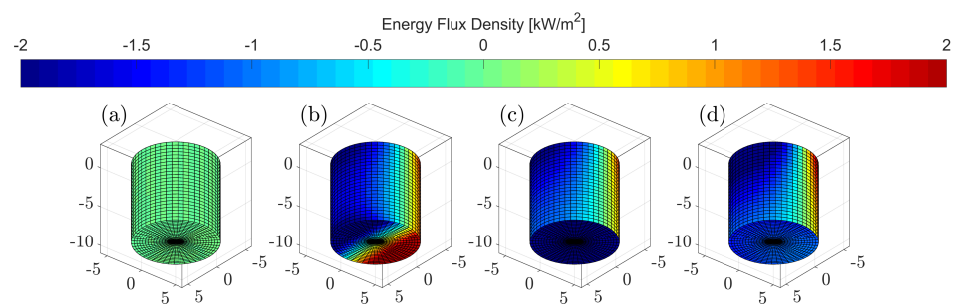

Figure 3. Energy flux surfaces on cylindrical geometry, showing monotonic ($T = 7.5$ s) cases for (**a**) diffracted wave field, (**b**) total wave field, and (**c**) total wave field with PTO damping in heave, and (**d**) the average total wave field for a wave spectrum with $H_s = 3.5$ m and $T_p = 7.5$ s with PTO damping in heave.

An experimental verification of the energy flux method would require measurements of normal relative velocities and pressures acting on the surfaces of the floating body, rendering a very challenging experimental setup. Instead, in this work, to verify the method, power capture is computed by integrating the energy flux over the surface (see Equation (5)). The predicted values are given in Table 1 alongside the predictions using the body motions and damping definition (see Equation (22)). The energy flux method correctly predicts zero power for cases (a) and (b) without PTO damping. For the damped cases (c), there is a negligible over-prediction and the wave spectrum with damping cases (d) agrees exactly. Thus, Table 1 shows that the power capture computed with the body motion approach and the energy flux method agree sufficiently, and, therefore, the energy flux model is verified for engineering applications.

Table 1. Comparison of expected (body motions) and predicted (energy flux surface) power for monotonic (a–c) and spectral (d) waves, as shown in Figure 3.

Case	Motions Prediction (kW)	Energy Flux Prediction (kW)
(a)	0	0
(b)	0	0
(c)	219.46	219.47
(d)	93.48	93.48

In the following subsections, the cases of a hinged barge and a pitching flap are used to illustrate further how the energy flux tool can be used to visualise the power surface of a moving body. Firstly, we show how the energy flux magnitude is affected by power take-off for a two-body hinged raft. Then, we use the tool to reveal why a flat pitching flap geometry is a more efficient captor than a curved flap geometry.

3.2. Hinged Barge

The second WEC example analysed in this work is a hinged barged, which is conceptually similar to the Mocean Energy WEC [30–33]. An exemplary twin-hulled hinged barge is utilised and shown in Figure 4. The forward hull, to the left of the figure, meets the incident waves. The total length of the barge is 60 m, the beam width is 8 m, the height is 4 m, and the draft is 2 m. A hinge located at the origin separates the two hulls. The motions of each hull are constrained at the hinge, producing a combined flex motion, from which power is extracted.
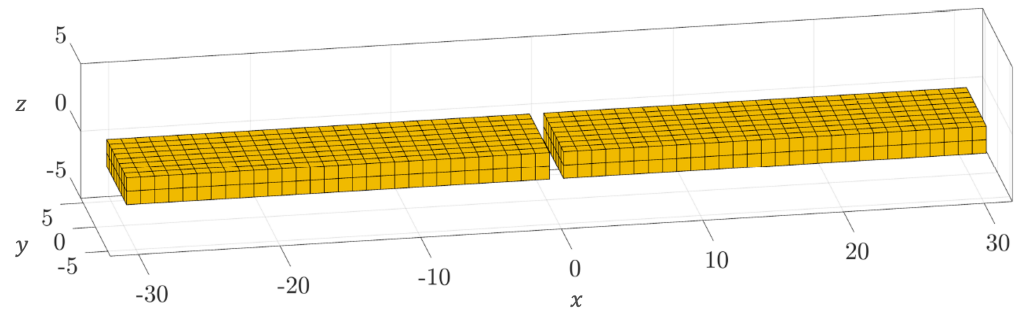
Figure 4. Twin-hulled hinged barge geometry.

Energy flux density surfaces are computed on the hinged barge for three different d_{PTO} values. The optimum damping coefficient d_{Opt} maximises the average power in a wave spectrum with $H_s = 3.5$ m and $T_p = 7.5$ s. In Figure 5, energy flux surfaces are shown for (a) underdamped (an order of magnitude below the optimum), (b) optimal damped, and (c) overdamped (an order of magnitude above the optimum) d_{PTO} values.
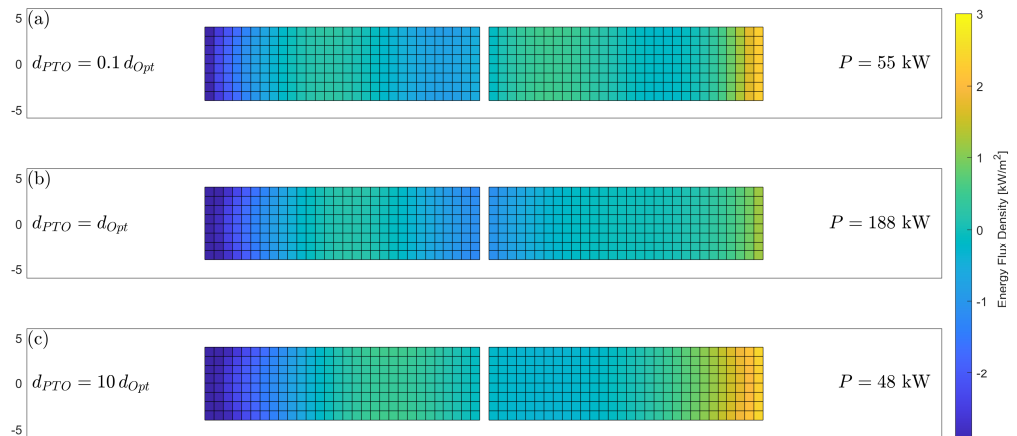
Figure 5. Average energy flux surfaces during a wave spectrum ($H_s = 3.5$ m, $T_p = 7.5$ s) on twin-hull hinged barge geometries, showing (**a**) underdamped power take-off, (**b**) optimum power take-off, (**c**) and overdamped power take-off.

The most obvious difference between the flux surfaces is the large yellow regions of positive energy flux at the end of the aft hull for the sub-optimal damped cases, which is most pronounced for the overdamped case (c), meaning more/larger waves are radiated here compared to the optimum (b). It also appears that as d_{PTO} increases so does the wave absorption at the front of the WEC. However, travelling inwards to the hinge at the centre of the device, there are regions of positive energy flux (power lost) for the sub-optimal cases, whereas for $d_{PTO} = d_{Opt}$ (b), power is absorbed on both sides of the hinge. Figure 5 highlights the usefulness of the tool to visualise the effect of different damping strategies on energy absorption throughout the hinged barge device.

3.3. Pitching Flaps

Lastly, the case of a pitching flap is analysed. In this example, two geometrically similar pitching flap configurations are compared, one with a flat surface, representative of the Oyster device [34,35], and one with a curved surface, similar to the CCell device [36], as shown in Figure 6a and Figure 6b, respectively.
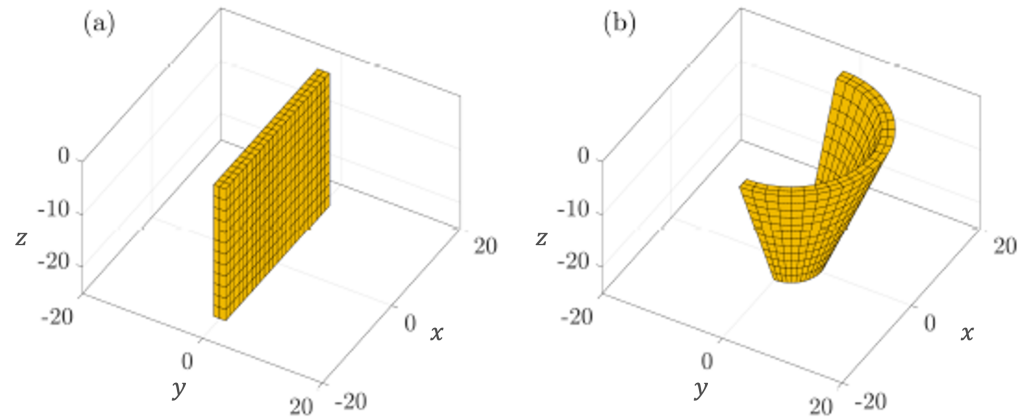

Figure 6. Geometries for (**a**) flat and (**b**) curved pitching flap WECs.

Optimised d_{PTO} values, for each configuration, are applied to the pitching motion. The resulting power RAO curves are shown in Figure 7. We see similar resonant peaks of 890 kW/m^2 at 9.4 s and 900 kW/m^2 at 9 s for the flat and curved flap, respectively. The flat flap has a much broader bandwidth than the curved flap. The average power in a wave spectrum with $H_s = 3.5$ m and $T_p = 7.5$ s is 840 kW and 570 kW for the flat and curved geometries, respectively. So, we ask why does this 32% power difference exist?
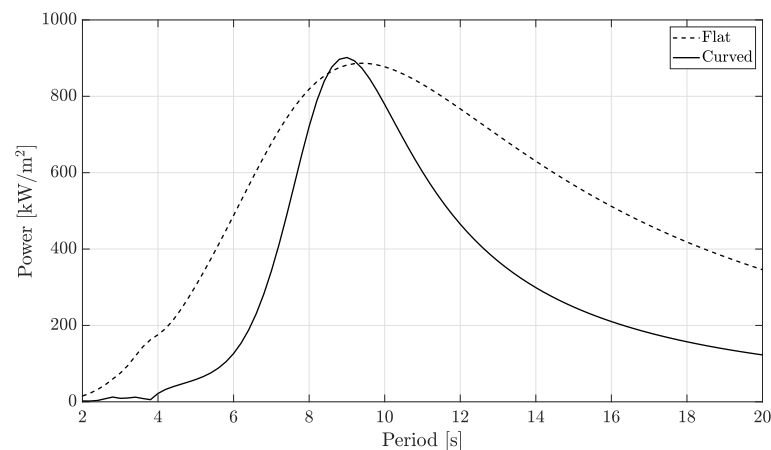
Figure 7. Power RAO curves for a flat and a curved pitching flap.

To answer this, the average energy flux surfaces are presented in Figure 8, where (a,b) and (c,d) show the flat and curved flap surfaces, respectively.

Qualitatively, the absorption surfaces for the flat (a) and curved (b) flaps are similar. However, when comparing the radiation sides, it is clear that the curved flap is radiating far more power back into the wave field. This explains the narrow-banded power RAO response that we observe in Figure 7 and the 32% power difference. Hence, the energy flux method proves to be a useful and cost-effective way to perform the power optimisation analysis of WECs with different geometric alternatives.
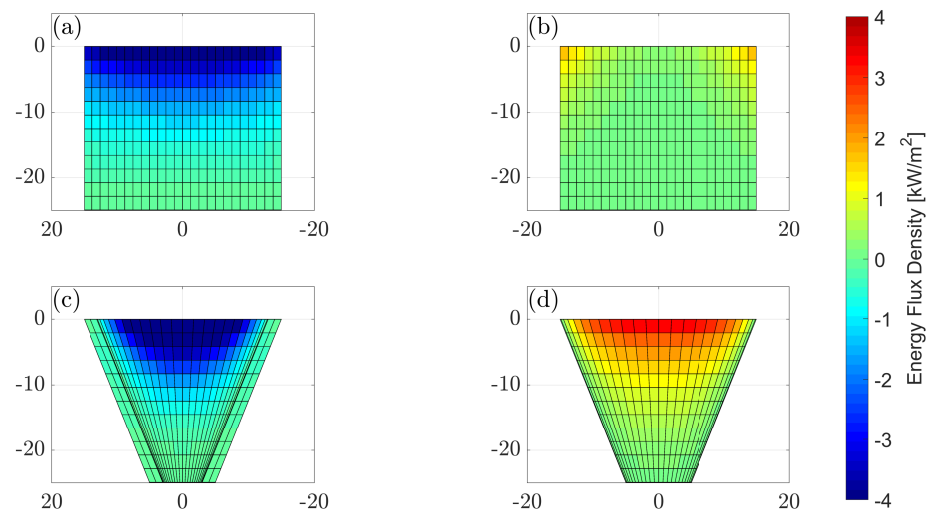
Figure 8. Average energy flux surfaces during a wave spectrum ($H_s = 3.5$ m and $T_p = 7.5$ s) on pitching flap geometries, showing flat-flap (**a**) absorption and (**b**) radiation surfaces and curved flap (**c**) absorption and (**d**) radiation surfaces.

4. Discussion

The proposed method to visualise the flow of power through the surface of a WEC is a novel engineering tool developed to enhance and optimise WEC power design. To the best knowledge of the authors, such a toolkit was not previously available in the literature. Although originally developed for WECs, the scope of application of the energy flux tool is vast, and other devices that interact with wave fields, for example floating wind turbines [37–39] or tidal turbines [40–42], could make use of the concepts presented in this paper.

Specifically for WECs, three aspects are demonstrated in this paper. First, as demonstrated with the heaving cylinder example, the tool is a highly accurate method that can be used to predict power capture. Secondly, as demonstrated with the hinged barge example, the method provides a quick and effective way to analyse energy absorption of a WEC subject to different damping strategies. Thirdly, as demonstrated with the pitching flap example, the tool can be used to find the optimum geometry of a WEC for power absorption.

Such a design engineering tool as the one presented in this work adds significant value to the design process of any WEC, particularly in early design stages, when high experimental costs can prevent WEC technology from being developed. Furthermore, it allows the analysis of the power absorption of WECs with different geometry designs. Finally, the proposed model offers the possibility of coupling the method to other design strategies, such as control engineering and structural design. It is the intention of the authors of this paper that this method contributes to the growth and development of WEC technology across the globe.

5. Conclusions

The fact that power flows from the fluid through the body surface as the product of dynamic pressure and normal velocity is not new to physics. However, it appears not to be widely recognised and has not been applied in an engineering tool. To aid early-stage design, an open-source software tool has been developed to visualise the flow of power (energy flux) from a wave field through the moving body surface of a WEC. The tool takes a frequency domain solution to compute the energy flux surface. This offers a practical method to understand how WECs are working and which parts are radiating or absorbing energy.

The main conclusions of the results presented in this work are summarised as follows:

1. The energy flux tool can be used to accurately predict power capture of a WEC.

2. The method can be used to assess the effect of different damping strategies on the power performance of a WEC.
3. The method can be used for the geometric optimisation of a WEC.

To evidence point 1, the method has been shown to accurately compute both peak power and average power in a wave spectrum compared with the conventional damped body motions approach. Subsequently, for point 2, the tool is used to visualise the hydrodynamic consequence of sub-optimal PTO damping for a twin-hulled hinged barge. This reveals that large portions of the aft body surface radiate power back into the wave field, which is most significant when the PTO is overdamped. Lastly, related to point 3, the performance of two pitching flap geometries is investigated: one flat and one curved, both geometrically comparable with similar peak power RAO values. However, the flat flap has a broader banded response, resulting in a 32% increase in average power capture during a wave spectrum with $H_s = 3.5$ m and $T_p = 7.5$ s, compared to the curved flap. By mapping the absorption and radiation energy flux surfaces for each flap, it is revealed that the curved flap radiates significantly more power back into the wave field due to it being curved.

We envisage future employment of the tool by developers to improve their device performance, increasing power absorption and making more efficient usage of materials. Optimisation could be carried out by using the energy flux tool to minimise surfaces which radiate significant portions of power back into the wave field. The tool could also be used to give a measure of efficiency by comparing the power absorbed to the power radiated. Future work will extend the tool to compute energy flux surfaces through a time domain solution.

References

1. Wave Energy Scotland. Driving the Development of Wave Energy Technology in Scotland. Available online: https://www.waveenergyscotland.co.uk (accessed on 24 September 2024).
2. WEC.0. Better Wave Energy Converters through Early-Stage Performance and Cost Design. Available online: http://wec0.eu/ (accessed on 24 September 2024).
3. Falnes, J.; Kurniawan, A. Fundamental formulae for wave-energy conversion. *R. Soci. Open Sci.* **2015**, *2*, 140305. [CrossRef] [PubMed]
4. Newman, J.N. The exciting forces of fixed bodies in waves. *J. Ship Res.* **1962**, *6*, 10–17. [CrossRef]
5. Newman, J.N. The interaction of stationary vessel with regular waves. In Proceedings of the 11th Symposium on Naval Hydrodynamics, London, UK, 28 March–2 April 1976; pp. 491–501.
6. Budal, K.; Falnes, J. A resonant point absorber of ocean-wave power. *Nature* **1975**, *256*, 478–479. [CrossRef]
7. Evans, D.V. A theory for wave-power absorption by oscillating bodies. *J. Fluid Mech.* **1976**, *77*, 1–25. [CrossRef]
8. McNatt, J.C. Cylindrical Linear Water Waves and their Application to the Wave-Body Problem. Ph.D. Thesis, The University of Edinburgh, Edinburgh, UK, 2015.

9. Journée, J.; Massie, W. *Offshore Hydromechanics*, 1st ed.; Delft University of Technology: Delft, The Netherlands, 2001.

10. Salter, S.H. Wave power. *Nature* **1974**, *249*, 720–724. [CrossRef]

11. Mei, C.C. Power extraction from water waves. *J. Ship Res.* **1976**, *20*, 63–66. [CrossRef]

12. Evans, D.; Jeffrey, D.; Salter, S.; Taylor, J. Submerged cylinder wave energy device: Theory and experiment. *Appl. Ocean Res.* **1979**, *1*, 3–12. [CrossRef]

13. Evans, D.V. Some analytic results for two and three dimensional wave-energy absorbers. In *Power from Sea Waves*; Academic Press, Inc.: London, UK, 1980; pp. 213–249.

14. Evans, D.V. Maximum wave-power absorption under motion constraints. *Appl. Ocean Res.* **1981**, *3*, 200–203. [CrossRef]

15. Budal, K. Theory for absorbtion of wave power by a system of interacting bodies. *J. Ship Res.* **1977**, *21*, 248–254. [CrossRef]

16. Folley, M. *Numerical Modelling of Wave Energy Converters—State of the Art Techniques for Single Devices and Arrays*; Elsevier: London, UK, 2016. [CrossRef]

17. Wypych, M.; Le-Ngoc, L.; Alexander, K.; Gardner, A. On the application of circular–cylindrical waves to ocean wave power absorption. *Ocean Eng.* **2012**, *40*, 69–75. [CrossRef]

18. Stansell, P.; Pizer, D.J. Maximum wave-power absorption by attenuating line absorbers under volume constraints. *Appl. Ocean Res.* **2013**, *40*, 83–93. [CrossRef]

19. Newman, J.N. Absorption of wave energy by elongated bodies. *Appl. Ocean Res.* **1979**, *1*, 189–196. [CrossRef]

20. Pizer, D.J. Maximum wave-power absorption of point absorbers under motion constraints. *Appl. Ocean Res.* **1993**, *15*, 227–234. [CrossRef]

21. Todalshaug, J.H. Practical limits to the power that can be captured from ocean waves by oscillating bodies. *Int. J. Mar. Energy* **2013**, *3–4*, e70–e81. [CrossRef]

22. Falnes, J. A review of wave-energy extraction. *Marine Struct.* **2007**, *20*, 185–201. [CrossRef]

23. Ermakov, A.; Marie, A.; Ringwood, J.V. Optimal Control of Pitch and Rotational Velocity for a Cyclorotor Wave Energy Device. *IEEE Trans. Sustain. Energy* **2022**, *13*, 1631–1640. [CrossRef]

24. Arredondo-Galeana, A.; Ermakov, A.; Shi, W.; Ringwood, J.V.; Brennan, F. Optimal control of wave cycloidal rotors with passively morphing foils: An analytical and numerical study. *Mar. Struct.* **2024**, *95*, 103597. [CrossRef]

25. MWave. A Water Wave and Wave Energy Converter Computation Package. [Software]. GitHub. Available online: https://github.com/cmcnatt/mwave (accessed on 24 September 2024).

26. Tuba Özkan-Haller, H.; Haller, M.C.; Cameron McNatt, J.; Porter, A.; Lenee-Bluhm, P. Analyses of Wave Scattering and Absorption Produced by WEC Arrays: Physical/Numerical Experiments and Model Assessment. In *Marine Renewable Energy: Resource Characterization and Physical Effects*; Yang, Z., Copping, A., Eds.; Springer International Publishing: Cham, Switzerland, 2017; pp. 71–97. [CrossRef]

27. McNatt, J.C.; Porter, A.; Ruehl, K. Comparison of Numerical Methods for Modeling the Wave Field Effects Generated by Individual Wave Energy Converters and Multiple Converter Wave Farms. *J. Mar. Sci. Eng.* **2020**, *8*, 168. [CrossRef]

28. Sheng, W.; Tapoglou, E.; Ma, X.; Taylor, C.; Dorrell, R.; Parsons, D.; Aggidis, G. Hydrodynamic studies of floating structures: Comparison of wave-structure interaction modelling. *Ocean Eng.* **2022**, *249*, 110878. [CrossRef]

29. Newman, J.; Malenica, U.; Ouled Housseine, C. Added mass and damping of structures with periodic angular shape. *J. Fluid Mech.* **2022**, *948*, R1. [CrossRef]

30. McNatt, J.C.; Retzler, C.H. The performance of the Mocean M100 wave energy converter described through numerical and physical modelling. *Int. Mar. Energy J.* **2020**, *3*, 11–19. [CrossRef]

31. Caio, A.; Davey, T.; McNatt, J.C. Preliminary hydrodynamic assessment of Mocean Energy's Blue Star WEC via fast turnaround physical model testing. In Proceedings of the 14th European Wave and Tidal Energy Conference, Plymouth, UK, 5–9 September 2021; under review. European Tidal and Wave Energy Conference.

32. Cummins, C.P.; Scarlett, G.T.; Windt, C. Numerical analysis of wave–structure interaction of regular waves with surface-piercing inclined plates. *J. Ocean Eng. Mar. Energy* **2022**, *8*, 99–115. [CrossRef]

33. Samuel, J.A.; Venugopal, V.; Retzler, C.; Ma, Q. Hydrodynamic Response of Mocean Wave Energy Converter in Extreme Waves. In Proceedings of the 15th European Wave and Tidal Energy Conference, Bilbao, Spain, 3–7 September 2023; Volume 15. [CrossRef]

34. Renzi, E.; Doherty, K.; Henry, A.; Dias, F. How does Oyster work? The simple interpretation of Oyster mathematics. *Eur. J. Mech.—B/Fluids* **2014**, *47*, 124–131. [CrossRef]

35. Choiniere, M.; Davis, J.; Nguyen, N.; Tom, N.; Fowler, M.; Thiagarajan, K. Hydrodynamics and load shedding behavior of a variable-geometry oscillating surge wave energy converter (OSWEC). *Renew. Energy* **2022**, *194*, 875–884. [CrossRef]

36. Hillis, A.; Sell, N.; Chandel, D.; Plummer, A. Control of the CCell Oscillating Surge Wave Energy Converter. *IFAC-PapersOnLine* **2017**, *50*, 14686–14691. [CrossRef]

37. Jonkman, J.M.; Matha, D. Dynamics of offshore floating wind turbines—Analysis of three concepts. *Wind Energy* **2011**, *14*, 557–569. [CrossRef]

38. Arredondo-Galeana, A.; Brennan, F. Floating Offshore Vertical Axis Wind Turbines: Opportunities, Challenges and Way Forward. *Energies* **2021**, *14*, 8000. [CrossRef]

39. Zeng, X.; Shao, Y.; Feng, X.; Xu, K.; Jin, R.; Li, H. Nonlinear hydrodynamics of floating offshore wind turbines: A review. *Renew. Sustain. Energy Rev.* **2024**, *191*, 114092. [CrossRef]

40. Scarlett, G.T.; Sellar, B.; van den Bremer, T.; Viola, I.M. Unsteady hydrodynamics of a full-scale tidal turbine operating in large wave conditions. *Renew. Energy* **2019**, *143*, 199–213. [CrossRef]
41. Scarlett, G.T.; Viola, I.M. Unsteady hydrodynamics of tidal turbine blades. *Renew. Energy* **2020**, *146*, 843–855. [CrossRef]
42. Zilic de Arcos, F.; Vogel, C.R.; Willden, R.H. A numerical study on the hydrodynamics of a floating tidal rotor under the combined effects of currents and waves. *Ocean Eng.* **2023**, *286*, 115612. [CrossRef]